Shape Sensing Using Two Outer Cores of Multicore Fiber and Optical Frequency Domain Reflectometer

Yanjie Meng, Cailing Fu, Chao Du, Lin Chen, Huajian Zhong, Pengfei Li, Baijie Xu, Bin Du, Jun He, and Yiping Wang, *Senior Member, IEEE*

***Abstract*—A method, i.e., vector projections, using two outer cores of multicore fiber without calibration and OFDR was proposed to realize three-dimensional (3D) shape sensing. A complement for apparent curvature vector method using three outer cores of multicore fiber was also proposed to determine the viable fiber cores arrangement for shape sensing. Compared with apparent curvature vector method, the vector projections method based on two outer cores of multicore fiber decreased the number of fiber cores, which eliminating the requirement for fiber cores arrangement. Based on these methods, a reconstructed shape with a higher accuracy was obtained based on integrating all fiber shape from all cores combinations. The maximum root-mean-square errors (RMSEs) of end position for the vector projections and apparent curvature vector method were 13.1 and 12.4 mm, while a higher accuracy, i.e., maximum RMSEs of 11.9 and 12.1 mm, was obtained based on the integrated fiber shapes.**

***Index Terms*—Bend sensing, multicore fiber, optical frequency domain reflectometer, shape sensing.**

I. Introduction

Shape sensing plays an important role in many fields, such as catheter tracking in medical care [1], soft robotics dynamically controlling [2], and proprioception of soft wearable devices in human-machine interfaces [3]. Existing methods to realize the shape sensing are usually based on optical camera imaging [4], ultrasound [5] and magnetic resonance image [1],[6], electromagnetic sensors [4] and optical waveguides [3], [7], [8]. Researchers have recently demonstrated various shape sensors using fiber Bragg grating (FBG) [9], Brillouin optical time domain analyzer [10], and phase-sensitive optical time domain reflectometry [11], optical frequency domain reflectometry (OFDR) [12] based on multicore fiber [13], fiber cluster [12], [14], [15], and substrate-attaching fibers [16] by analyzing differential strain distributions of the cross sections along the optical fiber. Shape sensing using OFDR [12] could achieve a higher spatial resolution, i.e., millimeter and even micrometer, to obtain an accurate strain distribution along the fiber. To reconstruct the fiber shape, two vital parameters, i.e., bending orientation and curvature recovered from the measured strain distribution using OFDR, should be substituted into Frenet-Serret Frame [13]. Recently, various methods and different core combinations have been demonstrated to recover the bending orientation and curvature. For example, Jason P. Moore *et al.* calculated the bending orientation and curvature based on three symmetrically arranged fiber cores using apparent curvature vector method [13]. Unfortunately, this method could not obtain accurate bending orientation in the case of non-symmetric cores arrangement [17]. Besides, by establishing an equation set about Bragg wavelength shift, temperature, axial strain, curvature and bending orientation of a four-core fiber, a least-square solution of reconstructed shape was obtained using Moore-Penrose pseudo-inverse matrix, which was a time-consuming calculation method [18], [19]. Moreover, Hou *et al.* obtained the curvature and bending orientation by using two off-diagonal outer-core FBGs and calibrated bending sensitivities [20]. However, the calibration process to determine bending sensitivities inevitably introduced systematic errors into reconstructed curvature vector, which would further impair the shape sensing accuracy.

In this paper, a method, i.e., vector projections, using two outer cores of multicore fiber without calibration and OFDR was proposed to realize 3D shape sensing. The response of shape sensing with the bending orientation from 0° to 360° was experimentally investigated. Meanwhile, a method using apparent curvature vector to determine what kind of arrangement of fiber cores could accurately calculate the bending orientation and curvature was also proposed. Moreover, the shape sensing accuracy of the two methods, i.e., vector projections and apparent curvature vector, was experimentally compared. Furthermore, a method based on integrating the obtained fiber shapes from all core combinations was also developed to improve the accuracy of the reconstructed fiber shape.

Manuscript received May 28, 2021; revised July 18, 2021; accepted July 26, 2021. Date of publication July 30, 2021; date of current version October 18, 2021. This work was supported in part by the National Natural Science Foundation of China under Grants 61905155 and U1913212, in part by the Natural Science Foundation of Guangdong Province under Grants 2019B1515120042, 2019A1515011393, and 2021A1515011925, and in part by the Shenzhen Key Laboratory of Photonic Devices and Sensing Systems for Internet of Things. *(Corresponding author: Cailing Fu.)*

The authors are with the Key Laboratory of Optoelectronic Devices and Systems of Ministry of Education/GuangDong Province, College of Physics and Optoelectronic Engineering, Shenzhen University, Shenzhen, Guangdong 518060, China, and also with the Shenzhen Key Laboratory of Photonic Devices and Sensing Systems for Internet of Things, Guangdong and Hong Kong Joint Research Centre for Optical Fibre Sensors, Shenzhen University, Shenzhen, Guangdong 518060, China (e-mail: mengyanjie2020@email.szu.edu.cn; fucailing@szu.edu.cn; 770839949@qq.com; 2060453065@email.szu.edu.cn; 1748996356@qq.com; lipengfei2022@163.com; 1900453046@email.szu.edu.cn; dubean@126.com; hejun07@szu.edu.cn; ypwang@szu.edu.cn).

Color versions of one or more figures in this article are available at https://doi.org/10.1109/JLT.2021.3100854.

Digital Object Identifier 10.1109/JLT.2021.3100854

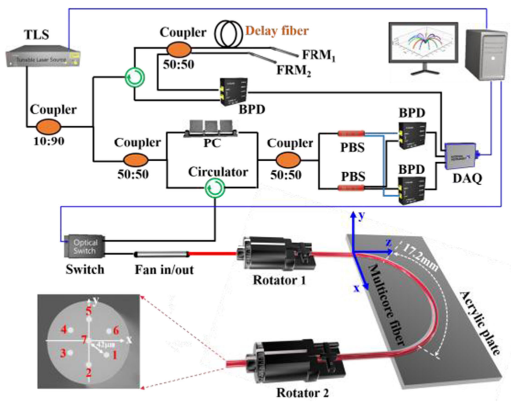

Fig. 1. Experimental setup based on OFDR for shape sensing using multicore fiber, i.e., seven-core fiber. Inset: scanning electron micrograph of the cross section of the employed multicore fiber and the defined local Cartesian coordinate system. TLS: tunable laser source; FRM: Faraday rotating mirror; BPD: balanced photo-detector; PC: polarization controller; PBS: polarization beam splitter; DAQ: data acquisition card.

II. Experimental Setup and Shape Sensing Principle

A. Experimental Setup

An experimental setup based on OFDR was built for shape sensing by measuring the distributed strain of each core along a multicore fiber, i.e., seven-core fiber (YOFC), as shown in Fig. 1. Light from a tunable laser source (TLS) was split into two paths, i.e., the auxiliary interferometer (AI) and main interferometer (MI), by a 10:90 coupler. The AI was comprised of two faraday rotating mirrors (FRMs) and a 100 m-long delay fiber, and the signal collected by a balanced photodetector (BPD) was used to trigger the data acquisition card (DAQ) with a sampling rate of 10 MS/s. In the MI, the beat signal generated by the sensing fiber, i.e., multicore fiber, was launched into two polarization beam splitters (PBSs) through a 50:50 coupler. The employed multicore fiber was spliced with a fan in/out spatial Mux/De-Mux coupler (YOFC), and a 1×8 mechanical optical switch was used to switch the light to each core with a time duration of 8 ms to finish the transition between two adjacent channels. Moreover, the multicore fiber was fixed by a pair of rotary fiber holders, i.e., rotator 1 and rotator 2, and embedded into a semicircular groove with a width and height of 1 and 2 mm, respectively, inducing a constant bending radius of 75 mm. To avoid the external force induced by the fiber holders, a 17.2 mm-long multicore fiber far from the fiber rotator was selected as the sensing section. The wavelength of the TLS was swept from 1530.00 to 1571.73 nm with a sweep rate of 10 nm/s, corresponding to a two-point spatial resolution of 19.8 μm. As shown in the inset of Fig. 1, the employed multicore fiber, i.e., seven-core fiber, has a central core, i.e., C_7, and six outer cores, i.e., C_m $(m = 1, 2 \ldots 6)$, arranged in a regular hexagon. The distance between two adjacent cores is 42 μm. In addition, the Cartesian coordinate system was established by setting the origin on the central core, i.e., C_7, of multicore fiber and referring to the line directing from the origin to an arbitrary point as the y-axis, and the z-axis is orthogonal to y-axis.

In the experiment, the reference signal was recorded when the multicore fiber was kept straight, while the measurement signal was acquired after putting the multicore fiber into the semicircular groove. The bending orientation was changed by rotating two holders simultaneously. The detailed process to calculate the distributed strain for shape sensing was as follows. The reference and measurement signal in the distance domain were acquired, then the inverse FFT was applied to obtain the spectrum of every sensing gauge with a length of 10.1 mm along the multicore fiber. And then the strain distribution could be obtained by multiplying the wavelength shift calculated from the cross-correlation between the reference and measurement spectrum by the calibrated strain coefficient, i.e., 6.67 $\mu\varepsilon$/GHz [21]. A computer with Intel Core(TM) i5-2520M @ 2.50 GHz and RAM of 4.0 GB was used to process data. Therefore, the overall strain distribution of the cross section along the multicore fiber could be obtained by repeating the process for each core.

B. Shape Sensing Principle Based on Two Outer Cores With Vector Projections Method

The Frenet-Serret Frame is defined by three mutually orthogonal space vectors, i.e., tangent vector $\boldsymbol{T}$, normal vector $\boldsymbol{N}$ and binormal vector $\boldsymbol{B}$, which are used to reconstruct the shape of the fiber [13]. The relationship between them can be expressed as

$$\frac{d}{ds}\begin{bmatrix}\boldsymbol{T}\\ \boldsymbol{N}\\ \boldsymbol{B}\end{bmatrix} = \begin{bmatrix}0 & \kappa & 0\\ -\kappa & 0 & \tau\\ 0 & -\tau & 0\end{bmatrix} \cdot \begin{bmatrix}\boldsymbol{T}\\ \boldsymbol{N}\\ \boldsymbol{B}\end{bmatrix} \tag{1}$$

where κ is the curvature, and τ is the torsion. The torsion is equal to the differential of bending orientation, i.e., θ_b, with respect to arc length, i.e., s, which is a measure of the rate of change of the osculating plane. It can be given by

$$\tau = \frac{d\theta_b(s)}{ds} \tag{2}$$

The (1) was discretized and accurately solved by the below matrix exponential,

$$[\boldsymbol{T}\ \boldsymbol{N}\ \boldsymbol{B}]_{\xi} = [\boldsymbol{T}\ \boldsymbol{N}\ \boldsymbol{B}]_{\xi-1} * e^{\begin{bmatrix}0 & \kappa & 0\\ -\kappa & 0 & \tau\\ 0 & -\tau & 0\end{bmatrix} * \Delta s} \tag{3}$$

where $[\boldsymbol{T}\boldsymbol{N}\boldsymbol{B}]_{\xi}$ and $[\boldsymbol{T}\boldsymbol{N}\boldsymbol{B}]_{\xi-1}$ are Ferret frame vectors of two consecutive points, i.e., ξ and ξ-1, respectively, and Δs is the distance between them, as illustrated in the inset of Fig. 2(d). Each point, i.e., $\mathbf{r}(s)$, in the curve can be determined using tangent vector, i.e., $\boldsymbol{T}$, by

$$\mathbf{r}(s) = \sum_{\xi=0}^{s} \boldsymbol{T}(\xi) \cdot \Delta s + \mathbf{r}_0 \tag{4}$$

where $\mathbf{r_0}$ is the initial position at $s = 0$, and the initial value of $\mathbf{r_0}$ is set as (0, 0, 0). Thus, the fiber shape can be reconstructed by (3)–(4).

As we know, curvature vector, i.e., κ, can be used to characterize the bending state of three-dimensional (3D) curve, which is comprised of curvature, i.e., κ, and bending orientation, i.e., θ_b. And the curvature vector can be obtained by analyzing differential strain distributions of the cross section along the multicore fiber. Assuming that the fiber is a linearly elastic

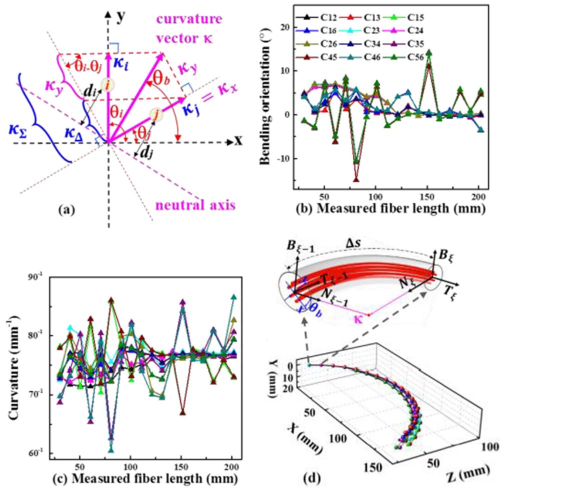

Fig. 2. (a) Schematic diagram of curvature vector reconstruction, including reconstruction of bending orientation and curvature, via vector projections method; Calculated (b) bending orientation, (c) curvature, and (d) reconstructed shape of the fiber embedded into a semicircular groove using different two cores combinations, i.e., C_{12}, C_{13} …, and C_{56}, of the multicore fiber.

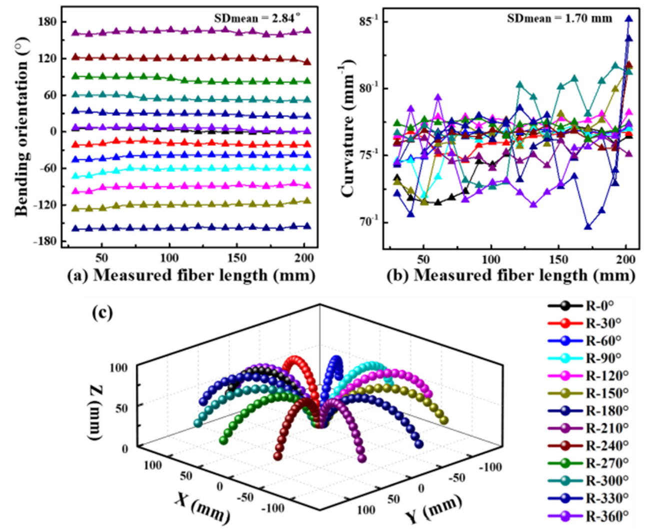

Fig. 3. Calculated (a) bending orientation, (b) curvature, and (c) reconstructed shape of the seven-core fiber embedded into a semicircular groove using combination of C_{12} via vector projections method when the fiber was rotated from 0° to 360° with a step of 30°, i.e., R-0°, R-30° …, and R-360°.

body [21] and cross sections remain plane and perpendicular to the neutral axis during deformation, the Euler-Bernoulli beam theory can be used to model the optical fiber bending [12]. The neutral axis, i.e., the center of the multicore fiber in Fig. 2(a), is passed through the geometrical centroid of the cross-section due to the homogeneity and symmetry of the multicore optical fiber. In this case, the strain of the central core is equal to zero, and then the strain of the outer core, i.e., ε_i, can be given by

$$\varepsilon_i = \frac{d_i}{R} = \kappa \cdot r_i \cos\left(\theta_b - \theta_i\right), \tag{5}$$

where d_i is the distance between C_i and neutral axis, R is bending radius, i.e., reciprocal of curvature κ, r_i is the distance between C_i and origin, and θ_i is the angle offset of C_i from x-axis. Note that the temperature and axial force would induce the same wavelength shift for all fiber cores, which makes the calculated strain of the center core is inequivalent to zero, resulting in the accuracy error for the reconstructed shape. The errors can be eliminated by subtracting the wavelength shift of the center core [18].

According to (5), the projection of curvature vector into the base vector pointing from the origin to outer C_i, can be given by

$$\kappa_i = \kappa \cdot \cos\left(\theta_b - \theta_i\right) = \frac{\varepsilon_i}{r_i}. \tag{6}$$

This indicated that the curvature vector could be reconstructed by two linearly independent projection vectors, which means that the selected two outer cores are not collinear with the central core. Thus, the available combination of two outer cores, i.e., C_{12}, C_{13}, C_{15}, C_{16}, C_{23}, C_{24}, C_{25}, C_{34}, C_{35}, C_{45}, C_{46}, and C_{56}, can be used to reconstruct the curvature vector by vector projections method, where C_{12} is the combination of C_1 and C_2.

As shown in Fig. 2(a), two outer cores, i.e., C_i and C_j, are arbitrarily selected, and the curvature vector i.e., κ, can be calculated by

$$\kappa = \sqrt{\kappa_x^2 + \kappa_y^2}, \tag{7}$$

$$\theta_b = \arctan\left(\frac{\kappa_y}{k_x}\right) + \theta_j, \tag{8}$$

where θ_j is the angle offset of C_j from x-axis, and

$$\kappa_x = \kappa_j = \frac{\varepsilon_j}{r_j}, \tag{9}$$

$$\kappa_y = \kappa_\Sigma - \kappa_\Delta = \frac{\kappa_i}{\sin\left(\theta_i - \theta_j\right)} - \frac{\kappa_j}{\tan\left(\theta_i - \theta_j\right)}. \tag{10}$$

where ε_j is the strain of C_j, and r_j is the distance between the C_j and origin.

Substituting the strain of two outer cores, i.e., ε_i and ε_j, into (6)–(10), the bending orientation and curvature of every sensing gauge along the fiber can be recovered, as illustrated in Figs. 2(b) and 2(c), respectively. Finally, the multicore fiber shape is reconstructed by (2)–(4). The reconstructed multicore fiber shapes are illustrated in Fig. 2(d) by using different two cores combinations, i.e., C_{12}, C_{13} …, and C_{56}, via the proposed vector projections method.

To investigate the response of the shape sensing by the proposed vector projections method, two ends of the multicore fiber was simultaneously rotated from 0° to 360° with a step of 30°, i.e., R-0°, R-30° …, and R-360°. As shown in Fig. 3(a), bending orientations have a good agreement with experimental parameters by using the combination of C_{12}. Note that the profile of R-360° is almost coincided with R-0°. The maximum standard deviation (SD) is 3.91°, occurring in R-270° while the mean SD, i.e., SD_{mean}, is 2.84°. As shown in Fig. 3(b), the bending radius, i.e., curvature, is fluctuated between 70 and 80 mm with a mean SD of 1.70 mm. Based on the local coordinate system shown in the inset of Fig. 1, the reconstructed fiber shapes under all rotation angles are illustrated in Fig. 3(c), indicating that the proposed vector projections method is feasible for shape sensing based on any combination of two outer cores which are not collinear with the central core.

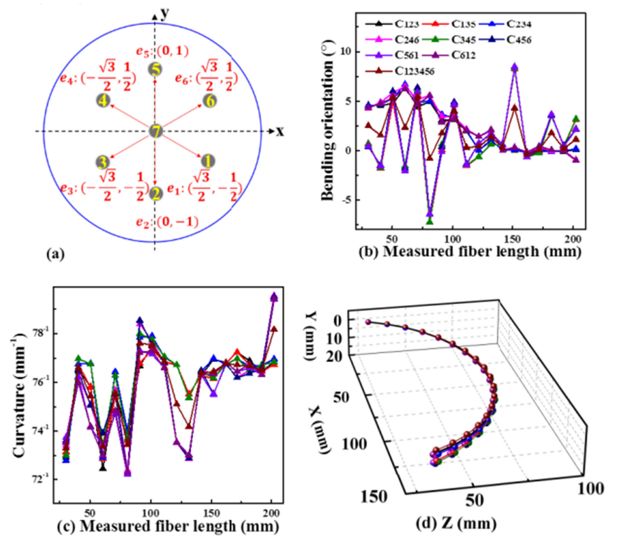

Fig. 4. (a) Base vector diagram of six outer cores for multicore fiber; Calculated (b) bending orientation, (c) curvature, and (d) reconstructed shape of fiber embedded into a semicircular groove using different three cores combinations, i.e., C_{123}, C_{135} …C_{612} and C_{123456}, of the multicore fiber via apparent curvature vector method.

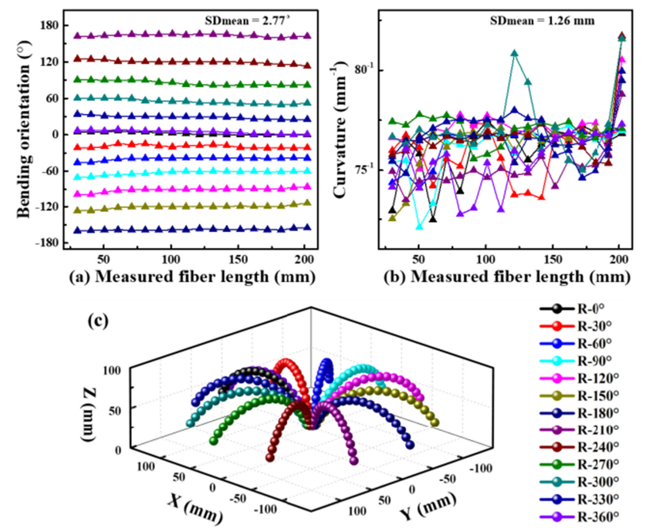

Fig. 5. Calculated (a) bending orientation, (b) curvature, and (c) reconstructed shape of fiber embedded into a semicircular groove using combination of core1, core2 and core3, i.e., C_{123}, via apparent curvature vector method when the fiber was rotated from 0° to 360° with a step of 30°, i.e., R-0°, R-30° …, and R-360°.

C. Complement for Apparent Curvature Vector Method

According to Ref. [13], apparent curvature vector method can reduce the error of reconstruction curvature vector induced by inaccurate measured strain distributions of fiber cross-section. The apparent curvature vector, i.e., $\boldsymbol{\kappa}_{app}$, is defined by

$$\boldsymbol{\kappa}_{app} = \left(-\sum_{i=1}^{N} \frac{\varepsilon_i}{r_i} cos\theta_i,\ -\sum_{i=1}^{N} \frac{\varepsilon_i}{r_i} sin\theta_i \right), \tag{11}$$

where N is the number of cores used for shape sensing. When the cores are arranged symmetrically or asymmetrically, the curvature, i.e., κ, can be given by [10], [17]

$$\kappa = \frac{\sqrt{\left(\sum_{i=1}^{N} \frac{\varepsilon_i}{r_i} cos\theta_i\right)^2 + \left(\sum_{i=1}^{N} \frac{\varepsilon_i}{r_i} sin\theta_i\right)^2}}{\sqrt{\left(\sum_{i=1}^{N} \cos(\theta_b - \theta_i)\ cos\theta_i\right)^2 + \left(\sum_{i=1}^{N} \cos(\theta_b - \theta_i)\ sin\theta_i\right)^2}}. \tag{12}$$

When the cores are arranged symmetrically, the bending orientation can be calculated by

$$\theta_b = \arctan\left(\frac{\sum_{i=1}^{N} \frac{\varepsilon_i}{r_i} sin\theta_i}{\sum_{i=1}^{N} \frac{\varepsilon_i}{r_i} cos\theta_i}\right). \tag{13}$$

Even though the fiber cores are symmetric, like an arrangement of rectangle, we found that (12)–(13) are not applicable to curvature vector reconstruction. Thus, what kind of core combination can be used to reconstruct the curvature vector by apparent curvature vector method is discussed.

The multicore fiber, i.e., seven-core fiber, in Fig. 1 is also employed as an example, where the angle offset is 60 °. As shown in Fig. 4(a), the base vector for each outer cores, i.e., C_1, C_2 … and C_6, can be expressed as a unit vector. For an arbitrary curvature vector $\boldsymbol{\kappa}_{arb} = (\kappa_\eta, \kappa_\xi)$, its projection into a base vector $\boldsymbol{e}_i$ is expressed as:

$$\boldsymbol{\kappa}_{arb,i} = \frac{\boldsymbol{\kappa}_{arb} * \boldsymbol{e}_i}{|\boldsymbol{e}_i|} * \boldsymbol{e}_i. \tag{14}$$

The sum of projections for the selected M cores is

$$\boldsymbol{\kappa}_{sum} = \sum_{i=1}^{M} \boldsymbol{\kappa}_{arb,i}. \tag{15}$$

If $\boldsymbol{\kappa}_{sum}$ is equal to $\boldsymbol{\kappa}_{arb}$, the curvature vector can be calculated correctly. If not, it is necessary to re-select the core or adopt a new algorithm. This indicates that the available cores combinations, i.e., C_{123}, C_{135}, C_{234}, C_{246}, C_{345}, C_{456}, C_{561}, C_{612}, and C_{123456}, can be used to reconstruct the curvature vector by using (12)–(13), where C_{123} is the combination of C_1, C_2, and C_3.

As shown in Figs. 4(b) and 4(c), the bending orientation and curvature along the multicore fiber are recovered, respectively. As shown in Fig. 4(d), the multicore fiber shape is also reconstructed by using afore-mentioned combinations via the apparent curvature vector method. Note that a combination of four or five cores is failed to calculate curvature vector using this method. As shown in Fig. 5, the fiber shape under different rotation angles from 0° to 360° with a step of 30° using cores combination C_{123} are reconstructed. The mean SD of bending orientation is 2.77°, while the mean SD of bending radius is 1.26 mm. The complement for apparent curvature vector method is not only used to the seven-core fiber, but also to other types of multicore fiber with various core arrangements.

III. Comparison of Vector Projections and Apparent Curvature Vector Method

It is well known that error of the curvature vector deteriorate the reconstructed shape and make position errors accumulate gradually [18]. Therefore, the error of the end position can be

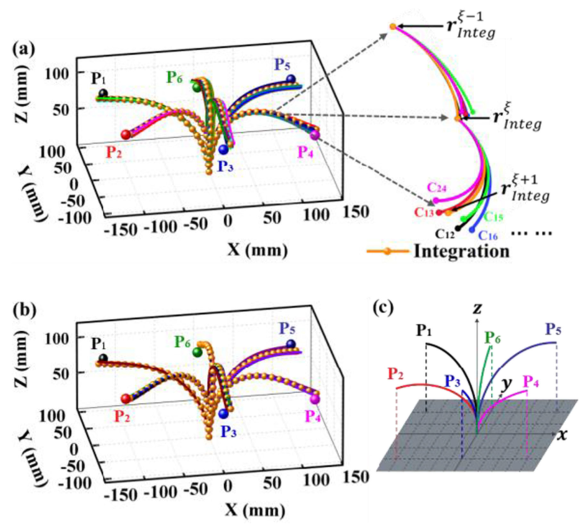

Fig. 6. Reconstructed shape using (a) vector projections, (b) apparent curvature vector method when six 3D shapes of the fiber were applied, where the end position was P_1, P_2 …, and P_6; (c) The measured value of the end position using coordinate paper and ruler.

TABLE I
END POSITION ERROR (MM) FOR VECTOR PROJECTIONS METHODS

Cores	P_1	P_2	P_3	P_4	P_5	P_6
C_{12}	8.0	9.5	10.0	10.5	13.4	13.6
C_{13}	8.3	10.2	9.6	10.7	13.8	11.7
C_{15}	9.6	10.4	8.7	11.3	14.4	13.0
C_{16}	8.7	9.1	11.8	5.1	16.4	11.4
C_{23}	13.1	9.8	14.4	8.7	10.0	12.0
C_{24}	9.6	10.0	15.3	9.4	10.4	14.9
C_{26}	9.5	9.4	11.1	9.2	15.7	11.8
C_{34}	9.0	9.0	9.1	7.2	8.9	12.1
C_{35}	9.6	9.8	15.5	8.8	7.8	12.8
C_{45}	10.2	9.7	12.7	10.2	11.1	13.5
C_{46}	9.9	9.0	7.1	1.6	16.7	12.5
C_{56}	9.0	9.2	13.5	9.3	14.8	11.3
RMSE	9.6	9.6	11.9	8.9	**13.1**	12.6
Integration	9.1	8.8	10.9	8.4	10.4	**11.9**

used to evaluate the performance of afore-mentioned methods, i.e., vector projections and apparent curvature vector method. To compare these two methods, the multicore fiber was shaped into six different 3D states, which were achieved by fixing the start point and then moving the end point to six different positions, i.e., P_1, P_2, P_3, P_4, P_5 and P_6, as illustrated in Fig. 6(c). The length of the employed multicore fiber is 200 mm. The actual end position, i.e, $\boldsymbol{r}_{gt}$, of the sensing multicore fiber can be accurately measured using a coordinate paper and ruler. Thus, the error of the end position of the six selected positions, i.e., P_i, for core combination, i.e., $C_{omb.j}$, is calculated by

$$error_{P_i}^{C_{omb.j}} = ||\boldsymbol{r}_{end} - \boldsymbol{r}_{gt}||, \tag{16}$$

where $\boldsymbol{r}_{end}$ is the value of the reconstructed end position by calculation. The reconstructed fiber shapes and errors of the end position for six different states, i.e., P_1, P_2, P_3, P_4, P_5 and P_6, using the afore-mentioned cores combinations in Figs. 2 and 4 are illustrated in Figs. 6(a) and 6(b), and Tables I and II, respectively.

TABLE II
END POSITION ERROR (MM) FOR APPARENT CURVATURE VECTOR METHOD

Cores	P_1	P_2	P_3	P_4	P_5	P_6
C_{123}	8.5	9.8	10.5	9.8	11.2	12.0
C_{135}	8.5	9.3	10.9	8.2	15.0	13.2
C_{234}	9.5	8.9	9.6	10.1	11.8	11.7
C_{246}	9.5	9.0	9.8	8.6	16.5	11.3
C_{345}	9.2	9.6	14.0	8.3	9.5	12.3
C_{456}	9.4	8.8	10.9	6.7	12.5	13.4
C_{561}	9.6	9.2	14.9	8.6	8.7	11.8
C_{612}	10.0	9.0	9.3	7.1	12.2	11.4
RMSE	9.3	9.2	11.4	8.5	**12.4**	12.2
Integration	9.3	8.8	10.9	8.4	10.9	**12.1**

To comprehensively evaluate the performance of these two methods, the root mean square error (RMSE) for each end position can be calculated by

$$\mathrm{RMSE}_{Pos.i} = \sqrt{\frac{\sum_{j=1}^{m} \left(error_{P_i}^{C_{omb.j}}\right)^2}{m}}, \tag{17}$$

where m is the number of cores combinations, i.e., $m = 12$ and 8 for vector projections and apparent curvature vector method, respectively. The maximum RMSEs are 13.1 and 12.4 mm for vector projections and apparent curvature vector, corresponding to the relative error of 6.55% and 6.20%, respectively, indicating that two methods have almost equal accuracy.

As shown in the inset of Fig. 6(a), there are slight differences between the fiber shapes reconstructed by different cores combinations due to measurement uncertainties [22], which also existed for the apparent curvature vector. To improve the accuracy of the reconstructed 3D fiber shape, a method based on integrating the obtained fiber shapes from all core combinations is proposed. As shown in the inset of Fig. 6(a), for the point ξ, different 3D positions $\boldsymbol{r}_{C_{omb.j}}^{\xi}$ are reconstructed by different cores combinations, and then the average of these positions, i.e., $\boldsymbol{r}_{Integ}^{\xi}$ is defined as the starting point to reckon the position $\boldsymbol{r}_{C_{omb.j}}^{\xi+1}$ of next point $\xi+1$. The integrated position for point $\xi+1$ is calculated as:

$$\boldsymbol{r}_{Integ}^{\xi+1} = \frac{\sum_{j=1}^{m} \left(\boldsymbol{r}_{Integ}^{\xi} + \boldsymbol{r}_{C_{omb.j}}^{\xi+1}\right)}{m}. \tag{18}$$

The integrated fiber shapes for the six states with improved accuracy were illustrated by the yellow dot line in Figs. 6(a) and 6(b) using the vector projections and apparent curvature vector method by repeating the afore-mentioned calculation process along the multicore fiber. As shown in Tables I and II, the maximum RMSEs of the two methods are reduced to 11.9 and 12.1 mm, respectively, indicating that the proposed method can improve the accuracy of the shape sensor.

IV. CONCLUSION

In conclusion, the 3D shape was experimentally reconstructed by using vector projections method based on two outer cores of multicore fiber and OFDR. Moreover, a complement for apparent curvature vector method using three cores combination of multicore fiber was proposed to determine the viable fiber cores arrangement for shape sensing. Almost equal accuracy, i.e., maximum RMSEs of 13.1 and 12.4 mm, were obtained for two methods, i.e., vector projections and apparent curvature vector, while the mean SDs of the bending orientation and radius were 2.84°, 1.70 mm and 2.77°, 1.26 mm, respectively. By averaging the calculated local positions of all cores combinations and then redefining the starting point, 3D fiber shapes with a higher accuracy, i.e., maximum RMSEs of 11.9 and 12.1 mm, were obtained. Compared with apparent curvature vector method, the vector projections method based on two outer cores of multicore fiber decreased the number of fiber cores for shape sensing, which is important for dynamic shape sensors.

References

[1] F. Parent *et al.*, "Intra-arterial image guidance with optical frequency domain reflectometry shape sensing," *IEEE Trans. Med. Imag.*, vol. 38, no. 2, pp. 482–492, Feb. 2019.

[2] R. K. Katzschmann *et al.*, "Dynamically closed-loop controlled soft robotic arm using a reduced order finite element model with state observer," in *Proc. IEEE Int. Conf. Soft Robot.*, 2019, pp. 717–724.

[3] H. D. Bai, S. Li, J. Barreiros, Y. Q. Tu, C. R. Pollock, and R. F. Shepherd, "Stretchable distributed fiber-optic sensors," *Sci.*, vol. 370, no. 6518, pp. 848–852, Nov. 2020.

[4] X. Ma, P. W. Y. Chiu, and Z. Li, "Real-time deformation sensing for flexible manipulators with bending and twisting," *IEEE Sensors J.*, vol. 18, no. 15, pp. 6412–6422, Aug. 2018.

[5] E. M. Boctor, M. A. Choti, E. C. Burdette, and R. J. Webster, "Three-dimensional ultrasound-guided robotic needle placement: An experimental evacuation," *Int. J. Med. Robot. Comput. Assist. Surg.*, vol. 4, no. 2, pp. 180–191, Jun. 2008.

[6] Y. L. Park *et al.*, "Real-time estimation of 3-D needle shape and deflection for MRI-guided interventions," *IEEE ASME Trans. Mechatron.*, vol. 15, no. 6, pp. 906–915, Dec. 2010.

[7] H. C. Zhao, K. O'Brien, S. Li, and R. F. Shepherd, "Optoelectronically innervated soft prosthetic hand via stretchable optical waveguides," *Sci. Robot.*, vol. 1, no. 1, Dec. 2016, Art. no. eaai7529.

[8] K. C. Galloway, Y. Chen, E. Templeton, B. Rife, I. S. Godage, and E. J. Barth, "Fiber optic shape sensing for soft robotics," *Soft Robot.*, vol. 6, no. 5, pp. 671–684, Oct. 2019.

[9] A. Wolf, A. Dostovalov, K. Bronnikov, and S. Babin, "Arrays of fiber Bragg gratings selectively inscribed in different cores of 7-core spun optical fiber by IR femtosecond laser pulses," *Opt. Exp.*, vol. 27, no. 10, pp. 13978–13990, May. 2019.

[10] Z. Y. Zhao, M. A. Soto, M. Tang, and L. Thevenaz, "Distributed shape sensing using brillouin scattering in multi-core fibers," *Opt. Exp.*, vol. 24, no. 22, pp. 25211–25223, Oct. 2016.

[11] L. Szostkiewicz *et al.*, "High-resolution distributed shape sensing using phase-sensitive optical time-domain reflectometry and multicore fibers," *Opt. Exp.*, vol. 27, no. 15, pp. 20763–20773, Jul. 2019.

[12] F. Parent *et al.*, "Enhancement of accuracy in shape sensing of surgical needles using optical frequency domain reflectometry in optical fibers," *Biomed. Opt. Exp.*, vol. 8, no. 4, pp. 2210–2221, Apr. 2017.

[13] J. P. Moore and M. D. Rogge, "Shape sensing using multi-core fiber optic cable and parametric curve solutions," *Opt. Exp.*, vol. 20, no. 3, pp. 2967–2973, Jan. 2012.

[14] S. Y. Zhao, J. W. Cui, C. Q. Yang, Z. Y. Ding, and J. B. Tan, "Simultaneous measurement of shape and temperature in the substrate-attaching-fibers sensing system," *IEEE Photon. J.*, vol. 9, no. 6, pp. 1–9, Dec. 2017.

[15] A. Issatayeva, A. Amantayeva, W. Blanc, D. Tosi, and C. Molardi, "Design and analysis of a fiber-optic sensing system for shape reconstruction of a minimally invasive surgical needle," *Sci. Rep.*, vol. 11, no. 1, pp. 8609–8609, Apr. 2021.

[16] M. Jang, J. S. Kim, S. H. Um, S. Yang, and J. Kim, "Ultra-high curvature sensors for multi-bend structures using fiber Bragg gratings," *Opt. Exp.*, vol. 27, no. 3, pp. 2074–2084, Feb. 2019.

[17] M. Rogge, "Shape sensing using a multi-core optical fiber having an arbitrary initial shape in the presence of extrinsic forces," US Patent 8 746 076 B2, Jun. 2014.

[18] F. Khan, A. Denasi, D. Barrera, J. Madrigal, S. Sales, and S. Misra, "Multicore optical fibers with Bragg gratings as shape sensor for flexible medical instruments," *IEEE Sensors J.*, vol. 19, no. 14, pp. 5878–5884, Jul. 2019.

[19] H. R. Zheng, Y. Jiang, M. Angelmahr, G. Flachenecker, H. W. Cai, and W. Schade, "Artificial neural network for the reduction of birefringence-induced errors in fiber shape sensors based on cladding waveguides gratings," *Opt. Lett.*, vol. 45, no. 7, pp. 1726–1729, Apr. 2020.

[20] M. X. Hou *et al.*, "Two-dimensional vector bending sensor based on seven-core fiber Bragg gratings," *Opt. Exp.*, vol. 26, no. 18, pp. 23770–23781, Sep. 2018.

[21] P. Antunes, H. Lima, J. Monteiro, and P. S. Andre, "Elastic constant measurement for standard and photosensitive single mode optical fibres," *Microw. Opt. Technol. Lett.*, vol. 50, no. 9, pp. 2467–2469, Sep. 2010.

[22] I. Floris, S. Sales, P. A. Calderon, and J. M. Adam, "Measurement uncertainty of multicore optical fiber sensors used to sense curvature and bending direction," *Measurement*, vol. 132, pp. 35–46, 2019.

Yanjie Meng was born in Guangling, China, in 1994. He received the B.Eng. degree in geomatics engineering from Southeast University, Nanjing, China, in 2016 and the M.S. degree from the China University of Mining and Technology, Xuzhou, China, in 2019. He is currently working toward the Ph.D. degree in optical engineering with Shenzhen University, Shenzhen, China. His main research interests include distributed optical fiber sensing and femtosecond laser processing.

Cailing Fu was born in Hubei, China, in 1989. She received the M.S. degree in optical engineering from the Wuhan Institute of Technology, Wuhan, China, in 2015 and the Ph.D. degree in optical engineering from Shenzhen University, Shenzhen, China, in 2018. From 2018 to 2020, she was with information and communication engineering of Shenzhen University, as a Post-doc Research Fellow. Since September 2020, she has been with Shenzhen University, as an Assistant Professor. She has authored or coauthored have more than 30 journal and conference papers. Her current research focuses on distributed optical fiber sensing technology.

Chao Du was born in Shanxi, China, in 1998. He received the B.S. degree from the School of Physics and Optoelectronic Engineering, Taiyuan University of Technology, Taiyuan, China, in 2020. He is currently working toward the M.S. degree in optical engineering with Shenzhen University, Shenzhen, China.

Lin Chen was born in Guangxi, China, in 1998. He received the B.S. degree from the Nanyang Institute of Technology, Singapore, in 2020. His current research interests include fiber gratings and femtosecond laser processing.

Huajian Zhong was born in Jiangxi, China, in 1998. He received the B.S. degree from the Changchun University of Science and Technology, Changchun, China, in 2020. His current research focuses on distributed optical sensing.

Pengfei Li was born in Henan, China, in 1991. She received the M.S. degree from the School of Physics and Engineering, Henan University of Science and Technology, Luoyang, China, in 2019. She is currently working toward the Ph.D. degree in optical engineering with Shenzhen University, Shenzhen, China.

Baijie Xu was born in Guangdong, China, in 1996. He received the B.Eng. degree in 2019 in optoelectronic information science and engineering from Shenzhen University, Shenzhen, China, where he is currently working toward the master's degree in optical engineering. His main research interests include optical fiber sensing and femtosecond laser processing.

Bin Du was born in Henan, China, in 1992. He received the B.S. degree in flight vehicle propulsion engineering from the School of Astronautics, Beihang University, Beijing, China, in 2016. His current research interests include fiber vibration and ultrasound sensor.

Jun He was born in Hubei, China, in 1985. He received the B.Eng. degree in electronic science and technology from Wuhan University, Wuhan, China, in 2006 and the Ph.D. degree in electrical engineering from the Institute of Semiconductors, Chinese Academy of Sciences, Beijing, China, in 2011. From 2011 to 2013, he was a Research Engineer with Huawei Technologies, Shenzhen, China. From 2013 to 2015, he was affiliated with Shenzhen University, Shenzhen, China, as a Postdoctoral Research Fellow. From 2015 to 2016, he was a Visiting Fellow with The University of New South Wales, Sydney, NSW, Australia. Since 2017, he has been an Assistant Professor with Shenzhen University. He has authored or coauthored four patent applications and more than 80 journal and conference papers. His current research interests include optical fiber sensors, fiber Bragg gratings, and fiber lasers. He is a Member of the Optical Society of America.

Yiping Wang (Senior Member, IEEE) was born in Chongqing, China, in 1971. He received the B.Eng. degree in precision instrument engineering from the Xi'an Institute of Technology, China, in 1995, and the M.S. and Ph.D. degrees in optical engineering from Chongqing University, Chongqing, China, in 2000 and 2003, respectively. From 2003 to 2005, he was a Postdoctoral Fellow with Shanghai Jiao Tong University, Shanghai, China. From 2005 to 2007, he was a Postdoctoral Fellow with Hong Kong Polytechnic University, Hong Kong. From 2007 to 2009, he was a Humboldt Research Fellow with the Institute of Photonic Technology (IPHT), Jena, Germany. From 2009 to 2011, he was a Marie Curie Fellow with the Optoelectronics Research Centre (ORC), University of Southampton, Southampton, U.K. Since 2012, he has been with Shenzhen University, Shenzhen, China, as a Distinguished Professor. He has authored or coauthored one book, 21 patent applications, and more than 240 journal and conference papers. His current research interests include optical fiber sensors, fiber gratings, and photonic crystal fibers. Prof. Wang is a Senior Member of the Optical Society of America and the Chinese Optical Society.